International Journal of Non-Linear Mechanics 92 (2017) 76–83

Contents lists available at ScienceDirect

International Journal of Non-Linear Mechanics

journal homepage: www.elsevier.com/locate/nlm

Bifurcation analysis of non-linear oscillators interacting via soft impacts

Joseph Páez Chávez[a,c], Piotr Brzeski[b,d,e,*], Przemyslaw Perlikowski[b]

[a] Center for Dynamics, Department of Mathematics, TU Dresden, D-01062 Dresden, Germany
[b] Division of Dynamics, Lodz University of Technology, Stefanowskiego 1/15, 90-924 Lodz, Poland
[c] Facultad de Ciencias Naturales y Matemáticas, Escuela Superior Politécnicadel Litoral, Km. 30.5 Via Perimetral, Guayaquil, Ecuador
[d] Potsdam Institute for Climate Impact Research (PIK), 14473 Potsdam, Germany
[e] Department of Physics, Humboldt University, 12489 Berlin, Germany

ARTICLE INFO

Keywords:
Duffing oscillator
Soft impact
Coexisting solutions
Hysteresis loop
Non-smooth dynamical system
Path-following

ABSTRACT

In this paper we present a bifurcation analysis of two periodically forced Duffing oscillators coupled via soft impact. The controlling parameters are the distance between the oscillators and the difference in the phase of the harmonic excitation. In our previous paper http://arXiv:1602.04214 (P. Brzeski et al. Controlling multistability in coupled systems with soft impacts [11]) we show that in the multistable system we are able to change the number of stable attractors and reduce the number of co-existing solutions via transient impacts. Now we perform a detailed path-following analysis to show the sequence of bifurcations which cause the destabilization of solutions when we decrease the distance between the oscillating systems. Our analysis shows that all solutions lose stability via grazing-induced bifurcations (period doubling, fold or torus bifurcations). The obtained results provide a deeper understanding of the mechanism of reduction of the multistability and confirmed that by adjusting the coupling parameters we are able to control the system dynamics.

1. Introduction

Systems interacting via impacts have attracted in recent years the attention of a growing number of researchers. In many mechanical systems, such as tooling machines, walking and hopping machines or gears, the motion of some elements is limited by a barrier or the other parts of a machine. In this paper we focus on mechanical interactions produced via soft impacts [1]. Therefore we assume a finite, nonzero contact time and a penetration of the colliding bodies. The contact forces are modeled using a linear [2,3], Hertzian [4,5] or other non-linear [6] spring and a viscous damper. To describe the behavior of such systems we introduce separate sets of smooth ODEs governing the system motion during the in-contact and out-of-contact stages.

Numerous investigations have been devoted to the analysis of various dynamical phenomena induced by impacts. The characteristic bifurcation for such systems is the grazing bifurcation, which can occur both for non-impacting and impacting solutions [7–10]. The grazing bifurcation occurs when the velocity of impact is zero and the trajectory just touches the boundary of impact. Hence, when passing the grazing point the change of a control parameter causes an appearance of a new impact, which takes place with zero impact velocity (a grazing impact). Grazing bifurcations may induce different events, such as sudden loss of stability, emergence of a new orbit or multiple orbits, a change in the period of the system's motion or creation of a chaotic attractor.

In this paper we carry out a bifurcation analysis of two non-linear oscillators interacting via transient impacts. We consider system of two identical oscillators and assume the interaction starts when the distance between them is sufficiently small. When the systems are uncoupled we observe multiple stable attractors for each subsystem, so the overall system is also multistable. Therefore, in this system we are able to change the number of stable attractors and reduce the multistability via transient impacts. This phenomenon has been introduced in our previous paper [11]. In this paper we investigate the mechanism that lies behind this phenomenon and show the sequence of bifurcations which cause the destabilization of solutions.

The paper is organized as follows. In Section 2 we introduce the model of two Duffing oscillators coupled via soft impacts. The description of continuation procedure is presented in Section 3. Then, in Section 4 we show the bifurcation analysis in one and two control parameters. Finally, in Section 5 the conclusions are given.

2. Physical model of the coupled Duffing oscillators and equations of motion

We investigate two coupled Duffing oscillators schematically presented in Fig. 1. The motion of the system is governed by the following

* Corresponding author at: Division of Dynamics, Lodz University of Technology, Stefanowskiego 1/15, 90-924 Lodz, Poland.
E-mail addresses: jpaez@espol.edu.ec (J.P. Chávez), piotr.brzeski@p.lodz.pl (P. Brzeski), przemyslaw.perlikowski@p.lodz.pl (P. Perlikowski).

http://dx.doi.org/10.1016/j.ijnonlinmec.2017.02.018
Received 23 December 2016; Accepted 13 February 2017
Available online 19 March 2017

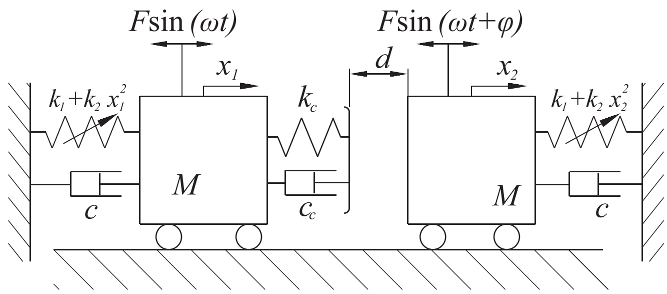

Fig. 1. Model of two discontinuously coupled Duffing oscillators.

equations:

$$M\ddot{x}_1 + k_1x_1 + k_2x_1^3 + c\dot{x}_1 + F_C = F\sin(\omega t), \tag{1}$$

$$M\ddot{x}_2 + k_1x_2 + k_2x_2^3 + c\dot{x}_2 - F_C = F\sin(\omega t+\varphi), \tag{2}$$

where a single over dot means differentiation with respect to the dimensional time. Here, F_C stands for the contact force generated by the discontinuous dissipative coupling, given by

$$F_C = \begin{cases} 0, & x_1 - x_2 < d, \\ k_c(x_1 - x_2 - d) + c_c(\dot{x}_1 - \dot{x}_2), & x_1 - x_2 \geq d. \end{cases} \tag{3}$$

In the present study, we will consider the equations of motion (1)–(2) in dimensionless form, according to the following formulas: $\tilde{x}_1 = \frac{x_1}{\ell_r}$, $\tilde{x}_2 = \frac{x_2}{\ell_r}$, $\tilde{\omega} = \frac{\omega}{\omega_r}$, $\tilde{t} = \omega_r t$, $\widetilde{M} = \frac{M}{m_r}$, $\tilde{k}_1 = \frac{k_1}{m_r\omega_r^2}$, $\tilde{k}_2 = \frac{k_2\ell_r^2}{m_r\omega_r^2}$, $\tilde{k}_c = \frac{k_c}{m_r\omega_r^2}$, $\tilde{c} = \frac{c}{m_r\omega_r}$, $\tilde{c}_c = \frac{c_c}{m_r\omega_r}$, $\tilde{d} = \frac{d}{\ell_r}$, $\tilde{F} = \frac{F}{m_r\ell_r\omega_r^2}$.
where $\ell_r = 1[m]$, $m_r = 1\,[kg]$ and $\omega_r = 1\,[rad/s]$ are the reference length, mass and frequency respectively. In the rest of the paper, the results will be presented considering the nondimensional variables and parameters introduced above. Nevertheless, all tildes will be omitted for the sake of simplicity. Similarly to our previous investigation [11] the controlling parameters will be the distance d between the subsystems and the phase shift in the excitation force of the second system φ.

3. The coupled Duffing oscillators as a piecewise-smooth dynamical system

The governing equations (1)–(2) can be studied in the framework of *piecewise-smooth dynamical systems* [12]. In this context, the state space is typically divided into disjoint subregions, each defining a particular operation mode of the system, where the system behavior is described by a smooth vector field. The boundaries of the subregions are defined by the zero-set of smooth scalar functions (known as *event functions*). Event functions are usually connected to physical instantaneous events, such as: impacts, switches, transitions from stick to slip motion, etc. When a trajectory crosses the boundary of a subregion, the vector field describing the system behavior is switched according to the governing laws of the system. A boundary crossing can be accurately detected by means of e.g. the standard MATLAB ODE solvers together with their built-in event location functionality [13,14], as implemented in [15].

To study the dynamics of the coupled Duffing oscillators, we employ path-following (continuation) method, which enables to systematically explore a model response subject to parameter variations [16], with focus on the detection of possible qualitative changes in the system dynamics (bifurcations). Computational tools specialized on path-following algorithms for piecewise-smooth dynamical systems have been developed in the past, such as SlideCont [17], TC-HAT [18] (see also [19–23] for some applications of this tool) and, more recently, COCO [24,25]. In the present work, we will apply COCO to study the non-linear behavior of the coupled Duffing oscillators. The next section will explain in detail the mathematical setup required to use the continuation software in order to carry out the numerical investigation.

3.1. Modeling of the coupled Duffing oscillators in COCO

In this paper we perform numerical investigation using path-following toolbox COCO (abbreviated form of Computational Continuation Core [24]). It is a MATLAB-based analysis and development platform for the numerical solution of continuation problems. The software provides the user with a set of toolboxes that covers, to a good extent, the functionality of available continuation packages, e.g. AUTO [26] and MATCONT [27]. A distinctive feature of COCO is, however, that it offers a general-purpose framework for the user to develop specialized toolboxes that can be constructed based on a number of generic COCO-routines, common across a large range of continuation problems.

In our investigation we will use the COCO-toolbox 'hspo', which extends and improves the functionalities of the software package TC-HAT [18], an AUTO-based application for continuation and bifurcation detection of periodic orbits of piecewise-smooth dynamical systems. The main differences between these two continuation toolboxes are discussed in detail in [25]. The mathematical setup required to apply the COCO-toolbox 'hspo' is the same as for TC-HAT. It requires to divide a piecewise-smooth periodic trajectory into smooth *segments*. Each segment is then characterized by a smooth vector field describing the system behavior in the segment and an event function that defines the terminal point of the segment, as explained at the beginning of Section 3. What follows,

$\lambda := (d, \varphi, \omega, F, M, k_1, k_2, c, k_c, c_c) \in \mathbb{R}_0^+ \times [0, 2\pi) \times (\mathbb{R}^+)^8$ and $u := (x_1, x_2, v_1, v_2)^T \in \mathbb{R}^4$ denotes the dimensionless parameters and state variables of system (1)–(2), respectively, where $\mathbb{R}_0^+$ stands for the set of nonnegative numbers. Below, we introduce the segments that are used for the numerical implementation in COCO.

No Contact (NC). This segment occurs when the oscillating masses move without touching each other, i.e. $(x_1 - x_2 < d$. In this segment the contact force F_C equals zero (see Fig. 1). The motion of the coupled Duffing oscillators during this regime is governed by the system of equations (cf. Eqs. (1)–(2))

$$u' = f_{\mathrm{NC}}(t, u, \lambda) := \begin{pmatrix} v_1 \\ v_2 \\ \frac{1}{M}(F\sin(\omega t) - k_1x_1 - k_2x_1^3 - cv_1) \\ \frac{1}{M}(F\sin(\omega t+\varphi) - k_1x_2 - k_2x_2^3 - cv_2) \end{pmatrix}, \tag{4}$$

where the prime symbol denotes differentiation with respect to the nondimensional time. This segment terminates when a transversal crossing with the impact boundary defined by

$$h_{\mathrm{IMP}}(u, \lambda) := x_1 - x_2 - d = 0$$

is detected, and the system switches to the *Contact* segment introduced below.

Contact (C). In this operation mode the oscillating masses are in contact, i.e. $x_1 - x_2 \geq d$, which gives rise to an additional force due to the discontinuous coupling defined by the spring-damper pair (k_c, c_c). The dynamics of the system in this operation mode is described by the equations (cf. Eqs. (1)–(2))

$$u' = f_{\mathrm{C}}(t, u, \lambda) := \begin{pmatrix} v_1 \\ v_2 \\ \frac{1}{M}(F\sin(\omega t) - k_1x_1 - k_2x_1^3 - cv_1 + \\ -(k_c(x_1 - x_2 - d) + c_c(v_1 - v_2))) \\ \frac{1}{M}(F\sin(\omega t+\varphi) - k_1x_2 - k_2x_2^3 - cv_2 + \\ +(k_c(x_1 - x_2 - d) + c_c(v_1 - v_2))) \end{pmatrix}, \tag{5}$$

with the terminal point being defined by the event $h_{\mathrm{IMP}}(u, \lambda) = 0$, after

Table 1
Segments defined for the numerical analysis of system (6)using the COCO-toolbox 'hspo'.

Index	Segment	Vector field	Event function
I_1	No Contact (NC)	f_{NC}	h_{IMP}
I_2	Contact (C)	f_{C}	h_{IMP}
I_3	Grazing Segment (GS)	f_{NC}	h_{GS}

which the contact between the two masses is lost and therefore the system switches to the *No Contact* mode defined previously.

Grazing Segment (GS). This segment is introduced in order to detect a grazing contact with the impact boundary $h_{\mathrm{IMP}}(u, \lambda) = 0$ during the *No Contact* mode. The system behavior during this segment is described by the ODE 4, and the end point of the segment is given by the equation:

$$h_{\mathrm{GS}}(u, \lambda) := v_1 - v_2 = 0.$$

This condition defines a point where the relative velocity between the oscillating masses becomes zero, which allows an accurate detection of grazing bifurcations by monitoring the function h_{IMP} evaluated at this point. Once a grazing bifurcation has been detected, adding the auxiliary boundary condition $h_{\mathrm{IMP}}(u, \lambda) = 0$ enable us to trace a curve in two control parameters at which a grazing contact takes place (see Section 4.3).

In Table 1 we show the segments introduced above with their corresponding vector fields and event functions. In addition, each segment is assigned with an index I_i, $i = 1, 2, 3$. In this setting, any periodic solution of the system can be fully defined by a sequence of segments $\{I_{\ell_j}\}_{j=1}^{K}$, referred to as *solution signature* [18], with $1 \le \ell_j \le 3$ and $K \in \mathbb{N}$. To conclude this section, we write below the governing equations of the coupled Duffing oscillators in compact form, in terms of the vector fields and event functions defined above

$$u' = \begin{cases} f_{\mathrm{NC}}(t, u, \lambda), & h_{\mathrm{IMP}}(u, \lambda) < 0, \\ f_{\mathrm{C}}(t, u, \lambda), & h_{\mathrm{IMP}}(u, \lambda) \ge 0. \end{cases} \tag{6}$$

4. Numerical results

In this section we carry out a detailed bifurcation analysis of the system via the continuation platform COCO, as explained in the previous section. Particular attention is given to the sequence of bifurcations which cause the destabilization of non-impacting solutions in the vicinity of grazing bifurcations. In the diagrams we describe each solution with the time of contact between the colliding oscillators. Such approach allows us to identify all non-impacting solutions for which the time of contact is zero.

4.1. Non-impacting dynamics of two Duffing oscillators

In Fig. 2 we show all non-impacting solutions of two coupled Duffing oscillators 6, computed for the following parameters values: $\omega = 1.3$, $d = 12$, $\varphi = 5.28$, $F = 1$, $M = 1$, $k_1 = 1$, $k_2 = 0.01$ $c = 0.05$, $k_c = 20$ and $c_c = 1$ (those values are fixed in the whole paper). The distance d and the phase shift φ are chosen in such a way that ensures no interaction between the oscillators. We observe two possible solutions for each isolated system. One with small and the second one with large amplitude of oscillations. They correspond to non-resonant and resonant periodic solutions, which typically co-exist close to the resonance frequency of the Duffing oscillator. The solutions are named according to the notation introduced in our previous article [11]: $L_1^1R_1^1$, $L_1^1R_1^2$, $L_1^2R_1^1$ and $L_1^2R_1^2$. The left- and right-hand side systems are named L_{pl}^{nl} and R_{pl}^{nl} respectively. The sub- and superscripts indicate the character of the periodic solution. The number of the attractor is denoted by ***nl*** (in case of multiple attractors of an isolated oscillator) and ***pl*** is the period of the given attractor with respect to the period of excitation (we assume that solutions are periodic). In our case ***nl*** is 1 (the small amplitude solution)

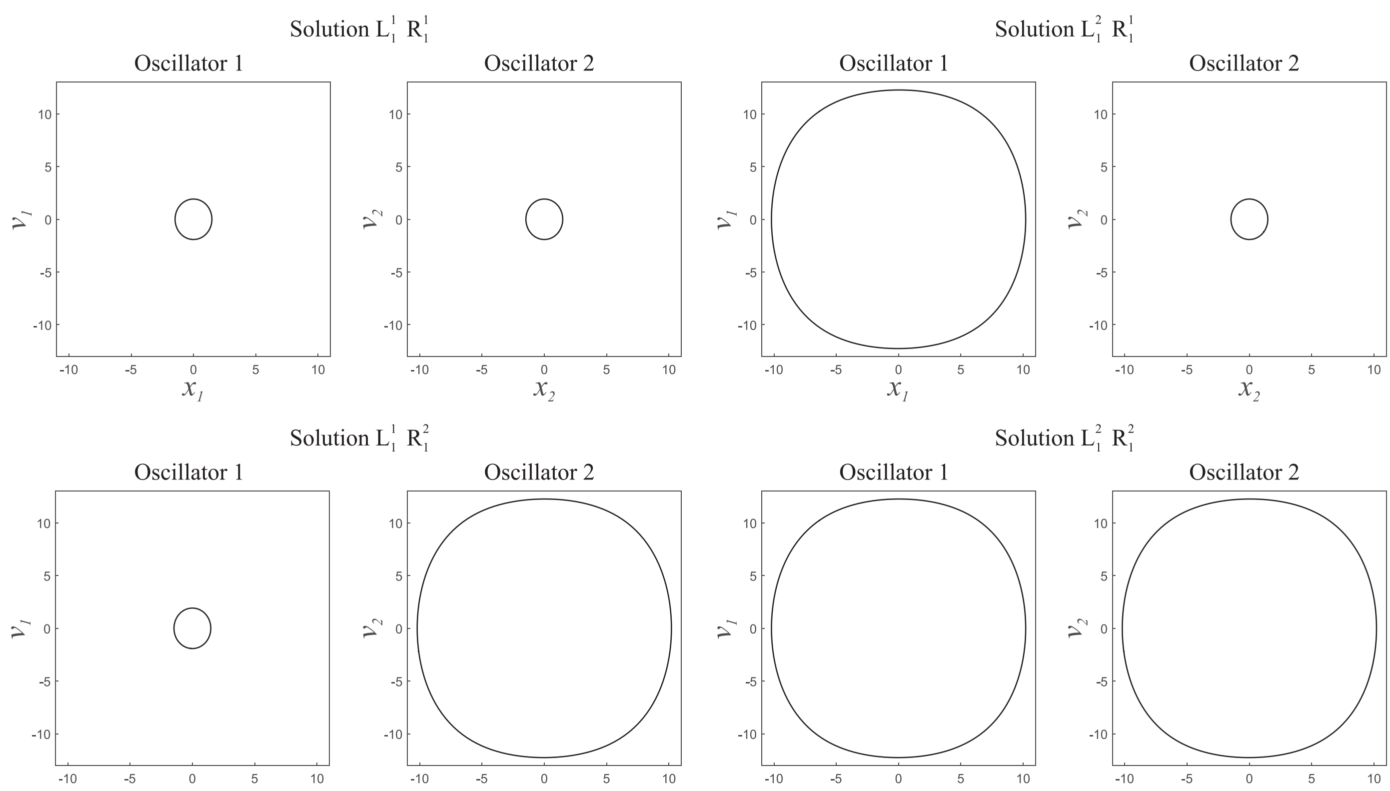

Fig. 2. Possible non-impacting solutions of two non-interacting Duffing oscillators (6), computed for the following parameters values: $\omega = 1.3$, $d = 12$, $\varphi = 5.28$, $F = 1$, $M = 1$, $k_1 = 1$, $k_2 = 0.01$ $c = 0.05$, $k_c = 20$ and $c_c = 1$.

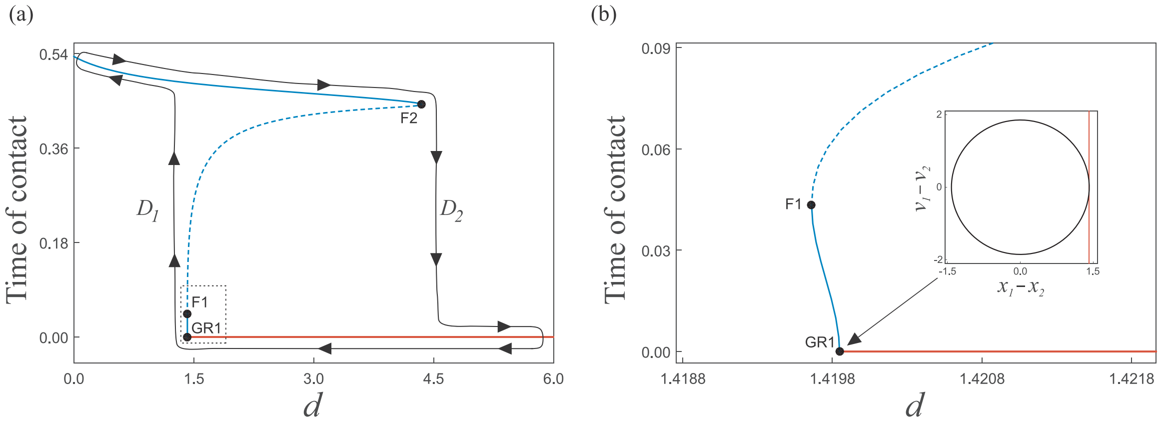

Fig. 3. (a) One-parameter continuation of the non-impacting solution $L_1^1R_1^1$ shown in Fig. 2 with respect to the distance d. The red segment of the bifurcation diagram corresponds to non-impacting while blue line depicts the impacting solution. The solid and dashed branches denote stable and unstable solutions, respectively. Bifurcation points are marked by black dots. The paths D_1-D_2 show schematically a hysteresis loop of the system. (b) Enlargement of the boxed region shown in panel (a). The inner diagram presents a periodic solution of the system at the grazing bifurcation GR1. Here, the vertical red line stands for the impact boundary $h_{\mathrm{IMP}}(u,\lambda) = x_1 - x_2 - d = 0$. (For interpretation of the references to color in this figure legend, the reader is referred to the web version of this article).

or 2 (the large amplitude solution), while pl is always 1 because both solutions have the same period as the excitation. The detailed description of notations for the periodic solutions and possible solutions of isolated Duffing oscillators are shown in [11]. In this paper we investigate in details the evolution of possible solutions via continuation methods.

4.2. One parameter bifurcation analysis

In Fig. 3 we show the result of the numerical continuation of the non-impacting solution $L_1^1R_1^1$ with respect to the distance d. Solid lines represent the stable solutions while dashed lines the unstable solutions. On the vertical axis we show the time of contact, which is the amount of time in which the two masses are in contact with each other during one period of the external excitation $\frac{2\pi}{\omega}$. Starting from large value of d we are on the red line that correspond to a non-impacting solution, with signature $\{I_3\}$. This means that the solution consists of the single segment *Grazing Segment* defined in Section 3.1, which is used to detect grazing bifurcations. As we reduce the distance d, we detect a grazing bifurcation GR1 at $d \approx 1.4198$, where the solution makes tangential contact with the impact boundary $h_{\mathrm{IMP}}(u,\lambda) = x_1 - x_2 - d = 0$ (see the inner plot of Fig. 3(b)). At this point, a solid blue branch emerges, corresponding to a stable impacting solution with signature $\{I_1, I_2\}$. That is, after the grazing bifurcation we have periodic solutions with two segments, one corresponding to non-impacting motion and one corresponding to impacting motion. If we decrease d further, we find a fold bifurcation F1 at $d \approx 1.4197$, which lies very close to the grazing point GR1. At F1 the solution loses stability (marked by the dashed line in Fig. 3(b)) and the blue branch turns in the increasing direction of d. From this point d increases until a second fold bifurcation F2 is detected at $d \approx 4.3481$, where the periodic solution regains stability, and therefore the blue branch becomes solid. Hereafter, d decreases, until the final point $d = 0$ is reached, below which the solutions of the system are physically meaningless. In Fig. 3(a), the paths D_1-D_2 show schematically a hysteresis loop of the system produced by the interplay between the two fold bifurcations found during the continuation, which is a typical mechanism by which a hysteretic behavior can appear, see e.g. [28], Section 8.2.

The results of numerical continuation of the second non-impacting solution $L_1^1R_1^2$ with respect to the distance d are shown in Fig. 4 As in the previous case, for large values of d the Duffing systems oscillate without interacting with each other. If d is decreased, a grazing bifurcation GR2 is detected at $d \approx 9.9437$, after which impacting motion begins. Very close to GR2, a torus bifurcation TR1 is encountered for

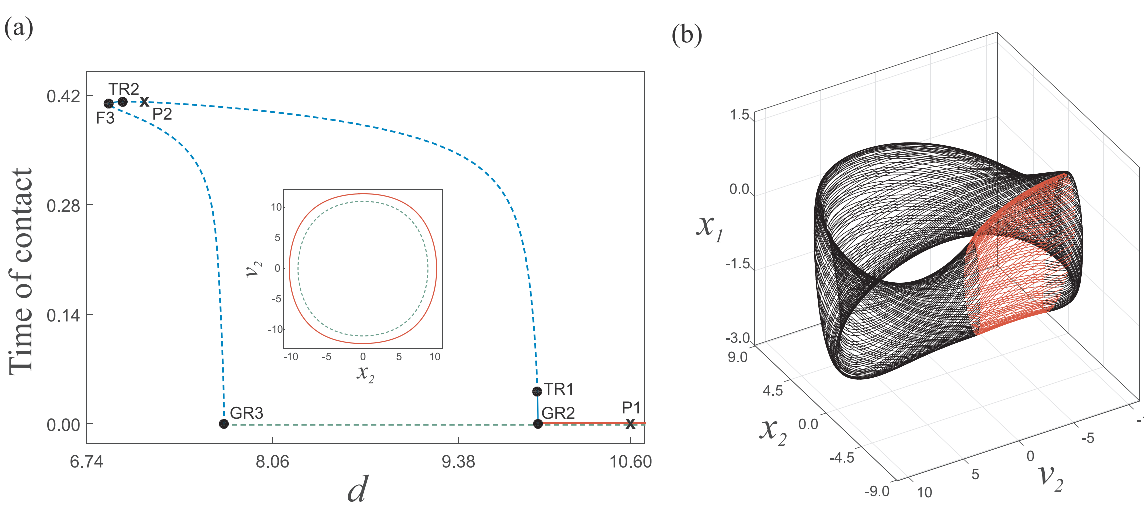

Fig. 4. (a) One-parameter continuation of the non-impacting solution $L_1^1R_1^2$ shown in Fig. 2 with respect to the distance d. The red and green segments of the bifurcation diagram correspond to non-impacting stable and unstable solutions, respectively. The blue line indicates the impacting solution. The inner set shows the corresponding stable (solid line) and unstable (dashed line) non-impacting solutions at the test point P1 ($d = 10.6$). (b) Quasiperiodic solution of the system near the torus bifurcation TR2 ($d \approx 6.9965$), computed at the test point P2 ($d = 7.15$). In this picture, the black and red colors mark the trajectory segments during non-impacting and impacting motion, respectively. (For interpretation of the references to color in this figure legend, the reader is referred to the web version of this article).

$d \approx 9.9399$. Here, a pair of complex conjugate Floquet multipliers of the periodic solution crosses the unit circle from the inside, and therefore stability is lost. If d is further decreased, another torus bifurcation TR2 at $d \approx 6.9965$ is found, where the unstable pair of Floquet multipliers enter again the unit circle, therefore the periodic solution becomes stable. Below TR2 we find a small window of stability which finishes at the fold bifurcation F3 encountered at $d \approx 6.8953$. From this point, a branch of unstable impacting solution goes to the increasing direction of parameter d. As d is increased along this branch, the time of contact decreases, until a grazing bifurcation GR3 is detected at $d \approx 7.7136$. It is important to note, however, that this is a grazing bifurcation of an unstable solution, which otherwise would not be detected via direct numerical integration. This allows us to trace a branch of unstable non-impacting solutions, marked by the green dashed line. This shows that in this case stable and unstable non-impacting solutions coexists in the system, as depicted in the inner set of Fig. 4(a), corresponding to the coexisting solutions at the test point P1 ($d = 10.6$). In panel (b), we show a quasiperiodic solution of system 6, computed at the test point P2 ($d = 7.15$). This quasiperiodic solution is produced by the torus bifurcation TR2 found before.

In Fig. 5 we show the result of the numerical continuation of the non-impacting solution $L_1^2R_1^1$ with respect to the distance d. For large values of d there is no interaction between Duffing systems. If d is decreased, a grazing bifurcation GR4 is detected at $d \approx 11.6562$, after which impacting motion begins. Very close to GR4, a torus bifurcation TR3 is encountered at $d \approx 11.6514$, where the solution loses stability. As shown in the inner window in Fig. 5(a), as the distance d is further decreased, a fold bifurcation F4 is detected at $d \approx 11.6361$, after which a total number of 3 Floquet multipliers lie outside the unit circle. However, as we trace the unstable branch further, we find another torus bifurcation TR4 for $d \approx 11.6734$, where a pair of Floquet multipliers enter the unit circle and leaves only one unstable multiplier. As we increase d, a fold bifurcation F5 at $d \approx 12.4466$ occurs, which in principle may help the solution regain stability. However, a closer look at the Floquet multipliers reveal that this is not the case, but at F5 another real multiplier crosses the unit circle from the inside, and therefore the stability of the periodic solution does not change. The solution branch now turns in the decreasing direction of d, and after a large excursion another fold bifurcation F6 is detected at $d \approx 9.0212$, where one of the unstable real multipliers gets inside the unit circle, leaving one unstable multiplier. After this, a grazing bifurcation GR5 is found at $d \approx 9.0318$, after which a branch of non-impacting unstable solutions exists (shown in green color). In panel (b) of Fig. 5 we present the solution manifold around the fold bifurcation F4, shown in the inner set depicted in panel (a). Here, we can geometrically verify that F1 corresponds indeed to a turning point of the solution manifold. A similar behavior can be observed around the fold bifurcations F5 and F6.

The path-following with respect to distance d of the last periodic solution $L_1^2R_1^2$ is shown in Fig. 6 We also start calculations for large distance d, and when d is decreased, a grazing bifurcation GR6 is detected at $d \approx 9.2303$. Below this value, we find a small parameter window of stable impacting motion, which terminates at the period-doubling bifurcation PD1 found at $d \approx 9.1709$. From here on, the periodic orbit becomes unstable. This unstable solution is traced further via continuation in the decreasing direction of d, and a second period-doubling bifurcation PD2 is encountered for $d \approx 0.1624$, where the orbit regains stability, and remains so until the terminal point $d = 0$. As it is well-known, a period-doubling bifurcation gives rise to a solution with twice the period of the original orbit, and in this case we also investigated such orbits. In Fig. 6(b) we show a stable period-2 orbit (solid line) computed at the test point P3 ($d = 0.176$), which lies close to the period-doubling bifurcation PD2. The dashed curve represents the corresponding unstable period-1 solution computed at the same test point. By tracing the period-2 solution via COCO, several bifurcations are detected. One of them corresponds to a grazing bifurcation GR7 detected at $d \approx 0.9887$, where the period-2 orbit makes grazing contact with the impact boundary $h_{\mathrm{IMP}}(u, \lambda) = x_1 - x_2 - d = 0$, as can be seen in Fig. 6(c). If we trace this periodic solution further in the decreasing direction of d, a period-doubling bifurcation of the period-2 orbit is found at $d \approx 0.9645$ (PD5), which gives rise to solutions of four times the period of the original orbit. Such a (stable) period-4 orbit can be found close to the period-doubling bifurcation, for instance at the test point P4 ($d = 0.952$), as depicted in Fig. 6(d). The sequence of bifurcations encountered for the period-2 solution is as follows (see Fig. 6(a)): fold $d \approx 0.4379$ (F7), fold $d \approx 0.3563$ (F8), period-doubling $d \approx 0.3564$ (PD4), period-doubling $d \approx 0.9645$ (PD5), fold $d \approx 1.0530$ (F9), grazing $d \approx 0.9887$ (GR7), fold $d \approx 0.5130$ (F10), period-doubling $d \approx 0.5131$ (PD6), period-doubling $d \approx 9.1482$ (PD3).

In all of the considered cases we observe the stabilization of periodic solutions with impacts. Nevertheless, all impacting solutions lose stability in the grazing-induced bifurcations (torus, period doubling or fold bifurcation). Therefore, it is possible to chose the values of controlling parameters to avoid the co-existence of impacting and non-impacting solutions.

4.3. Two-parameter analysis of the impacting motion

To further explain the evolution of the solution $L_1^1R_1^1$ presented in Fig. 3 we perform the two-parameter continuation of the codimension-1

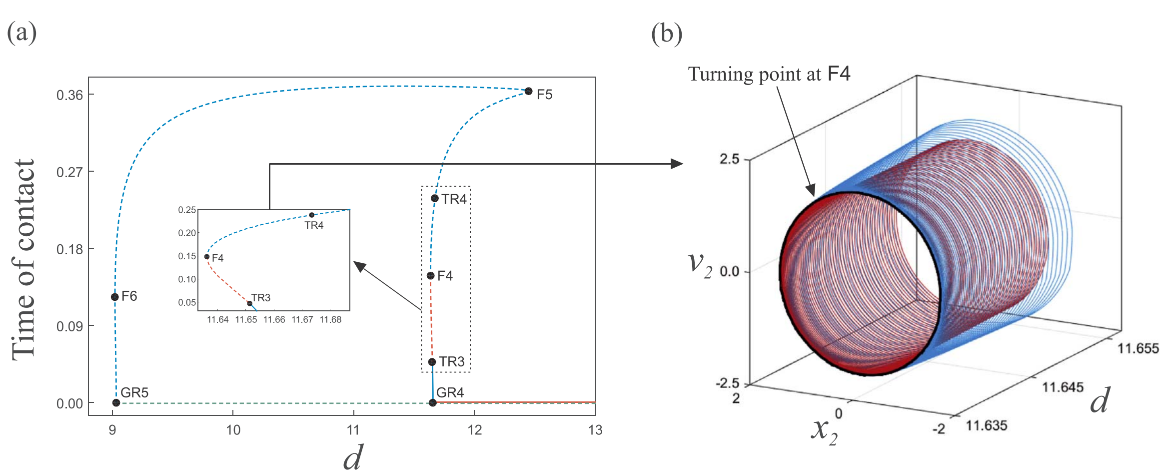

Fig. 5. (a) One-parameter continuation of the non-impacting solution $L_1^2R_1^1$ shown in Fig. 2 with respect to the distance d. (b) Solution manifold around the fold bifurcation F4 ($d \approx 11.6361$). The red and blue colors denote the solutions computed for the corresponding colored branches in the enlarged region shown in panel (a). The turning point of the solution manifold at F4 is plotted in black. (For interpretation of the references to color in this figure legend, the reader is referred to the web version of this article).

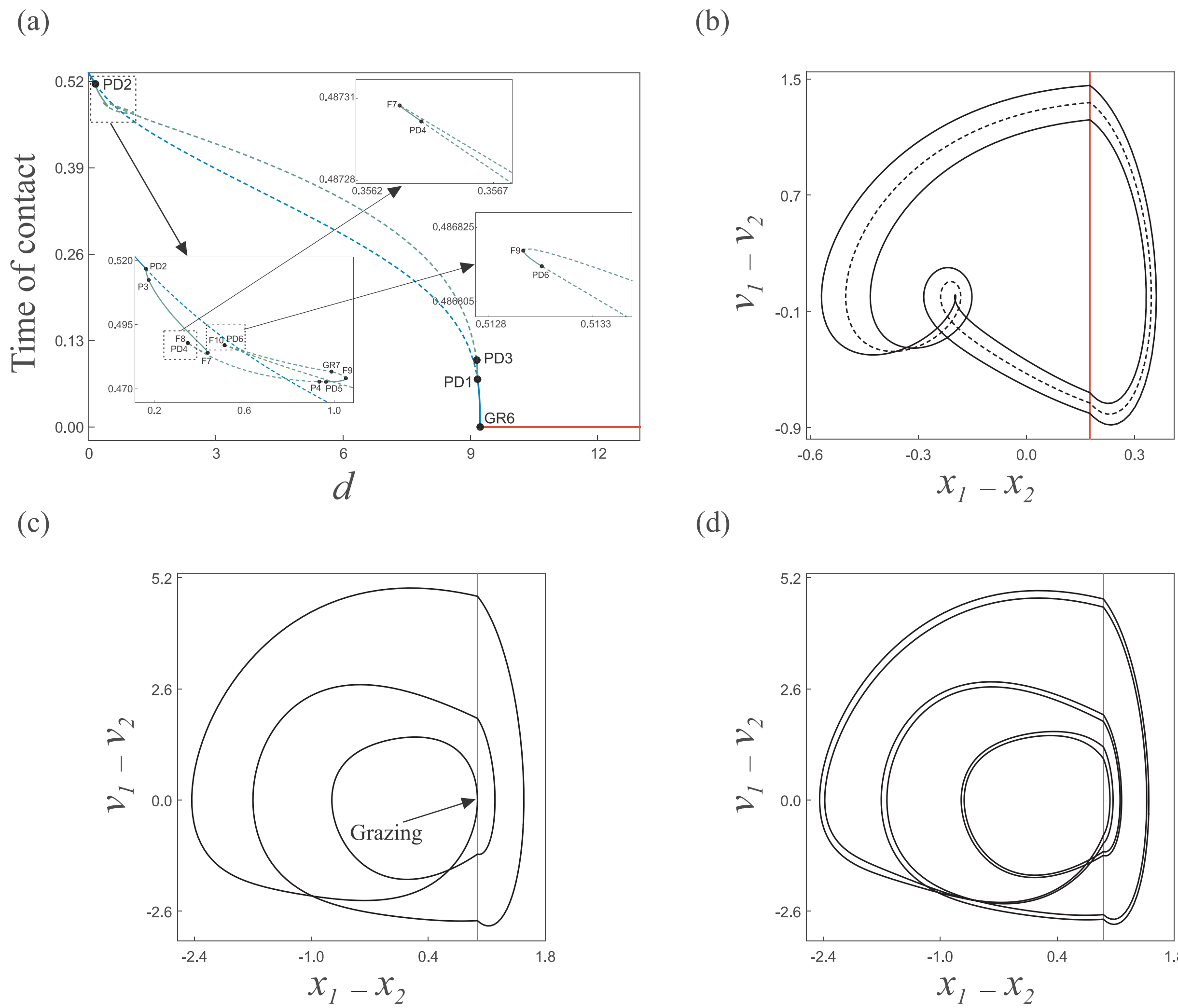

Fig. 6. (a) One-parameter continuation of the non-impacting solution $L_1^2R_1^2$ shown in Fig. 2 with respect to the distance d. The green segment stands for the continuation of a period-2 solution (see panel (b)) originating from the period-doubling bifurcation PD2 ($d \approx 0.1624$). (b) Period-1 (dashed line, unstable) and period-2 (solid line, stable) solutions computed at the test point P3 ($d = 0.176$) shown in panel (a), close to the period-doubling bifurcation PD2. (c) Period-2 orbit making grazing contact with the impact boundary $h_{\text{IMP}}(u, \lambda) = x_1 - x_2 - d = 0$ (red line), detected at GR7 ($d \approx 0.9887$). (d) Period-4 solution computed at the test point P4 ($d = 0.952$), which originates from the period-doubling bifurcation PD5 ($d \approx 0.9645$) shown in panel (a). (For interpretation of the references to color in this figure legend, the reader is referred to the web version of this article).

bifurcations GR1 (blue curve), F1 (red curve) and F2 (green curve) with respect to d and φ. The results are shown in Fig. 7. The red and blue curves of fold and grazing bifurcations nearly overlap. Hence, to show that there is a small distance between them we zoom them in the inner panel of subplot (a). In this picture we can verify the small distance between these two curves, which gives an indication that the fold bifurcation is being induced by the grazing phenomenon occurring in the system, which is a typical scenario for systems with soft impacts (see e.g. [19,21,29], Example 2.3). At $\varphi = 5.28$ there is a dashed vertical line which corresponds to the bifurcation scenario depicted in Fig. 3. The closed curve $D_1 - D_2$ shows schematically the hysteresis loop found for $\varphi = 5.28$, produced by the presence of the fold bifurcations F1 and F2. According to the two-parameter bifurcation diagram, small perturbations in the phase shift will preserve the hysteresis loop. However, for phase shifts below the critical point TP ($\varphi \approx 5.1051$), which corresponds to a turning point of the fold curve, the hysteresis loop disappears. This is verified in Fig. 7(b), where the continuation of the non-impacting solution $L_1^1R_1^1$ is shown for $\varphi = \frac{3\pi}{2}$. Here, only one fold bifurcation is detected (F11, $d \approx 2.0887$), corresponding to the intersection of the vertical line $\varphi = \frac{3\pi}{2}$ and the red fold curve shown in Fig. 7(a). Due to the symmetry in the system we observe the mirror reflection of this fold bifurcation curve on the left side of Fig. 7(a).

Now, let us describe in details the phenomena that occur due to the existence of the green branch. It corresponds to the two-parameter continuation of the fold point F2 found in Fig. 3. This fold curve, however, has itself a turning point (TP) which divides the branch into two parts that are dynamically separated. The continuation shown in Fig. 3 only shows one fold bifurcation found in the lower branch of the green fold curve. This separation is basically due to the hysteresis loop D_1-D_2 shown in Figs 3 and 7. For large values of d (gap), the masses move separately. If d decreases, at some point the solution hits the grazing curve (blue), shown in Fig. 7. If d decreases a little bit further, then the solution encounters the fold curve (red) and therefore the solution branch turns back. After this, d starts increasing, but with Duffing oscillators contacting each other. If d increases further, at some point the solution branch hits the green fold curve, which again makes the solution branch turn back, and from this point d decreases again. This is why we do not see a fold bifurcation on the upper part of the green curve (above the TP point) during the one-parameter continuation shown in Fig. 3.

In Fig. 8 we show the result of the two-parameter continuation of the grazing bifurcations GR1 (red curve), GR2 (green curve), GR4 (blue curve) and GR6 (black curve) found in our previous numerical investigations (see Figs.(3)–(6)). Here, we did not consider the grazing bifurcations GR3 and GR5 because those correspond to unstable solutions that in this case have no relevant influence in the system

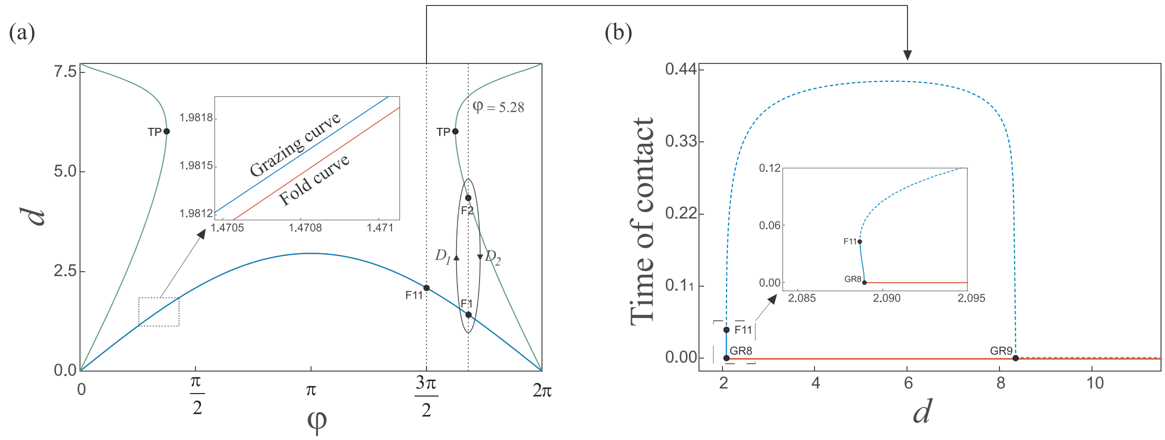

Fig. 7. (a) Two-parameter continuation of the codimension-1 bifurcations GR1 (blue curve), F1 (red curve) and F2 (green curve) found in Fig. 3 with respect to d and φ. The label TP stands for a turning point of the green fold curve. The closed curve D_1-D_2 shows schematically the hysteresis loop found in Fig. 3, produced by the presence of the fold bifurcations F1 and F2 for $\varphi = 5.28$. (b) One-parameter continuation of the non-impacting solution $L_1^1 R_1^1$ shown in Fig. 2 with respect to the distance d, for $\varphi = \frac{3\pi}{2}$. In this case, the hysteresis loop D_1-D_2 disappears. (For interpretation of the references to color in this figure legend, the reader is referred to the web version of this article).

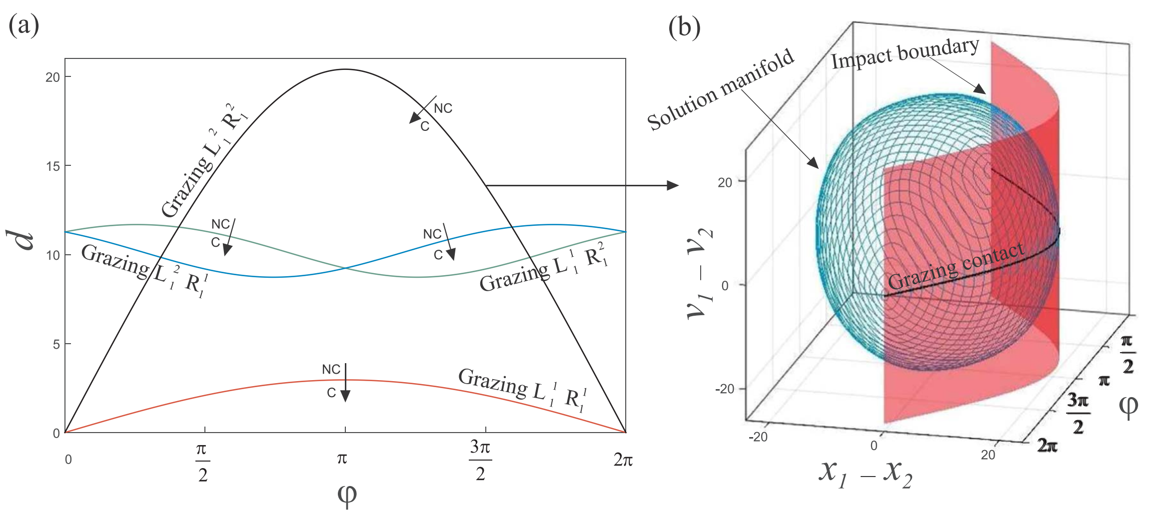

Fig. 8. (a) Two-parameter continuation of the grazing bifurcations GR1, GR2, GR4 and GR6 (see Figs.(3)–(6)) with respect to d and φ, corresponding to the non-impacting solutions $L_1^1 R_1^1$, $L_1^1 R_1^2$, $L_1^2 R_1^1$ and $L_1^2 R_1^2$, respectively. The arrows indicate the transition from non-impacting (NC) to impacting (C) motion. (b) Solution manifold computed along the grazing curve for $L_1^2 R_1^2$. Here, the red surface stands for the impact boundary $h_{\text{IMP}}(u, \lambda) = x_1 - x_2 - d(\varphi) = 0$, with $(\varphi, d(\varphi))$ on the grazing curve. The tangential contact between the solution manifold and the impact boundary is marked by a black curve on the surface. (For interpretation of the references to color in this figure legend, the reader is referred to the web version of this article.)

dynamics. Additionally we neglect the small region of existence of stable impacting solution shown in previous figure (within green lines). The two-parameter continuation is shown in Fig. 8(a), carried out in the φ-d plane. Each curve divides the control plane in two regions: one where the corresponding $L_1^m R_1^n$ orbit is non-impacting and one where $L_1^m R_1^n$ bifurcates to a narrow region of stable impacting motion. A transition from non-impacting (NC) to impacting behavior (C) is marked by an arrow in the picture. In Fig. 8(b) we show the solution manifold computed along the two-parameter continuation of the grazing bifurcation GR6 (black curve). The red surface represents the behavior of the impact boundary $h_{\text{IMP}}(u, \lambda) = x_1 - x_2 - d(\varphi) = 0$, with $(\varphi, d(\varphi))$ on the black grazing curve. In the picture, we can geometrically verify that the solution manifold makes tangential contact with the impact boundary, for every point along the grazing curve.

5. Conclusions

In this paper we present a path-following bifurcation analysis of the system that consists of two identical Duffing oscillators interacting via soft impacts. In our previous paper [11] we show that by changing the distance d and the phase shift φ of excitation we can control the dynamics of the system and ensure that both Duffing oscillators perform the desired type of non-impacting motion. Now, we extend the analysis to demonstrate the bifurcation scenarios which lie beneath the detected phenomena. Impacting systems, due to non-smoothness, cannot be analysed using classical path-following toolboxes, so we obtained all the stable and unstable branches using the continuation platform COCO [24].

When the subsystems are at large distance d there is no interaction between them. In such case there are four possible states of the overall system. We investigate the evolution and the bifurcation scenarios that lead to destabilization of these states. We show that for all considered non-impacting solutions a grazing bifurcation occurs with the decrease of the distance d. In this point the non-impacting solution disappears and a stable impacting solution emerges. However, when the distance d is further slightly decreased the impacting solution loses its stability in a grazing-induced bifurcation, i.e., period doubling, torus and fold bifurcation. In the case of the solution $L_1^1 R_1^1$ when further following the impacting solution we observe its stabilization after the second fold bifurcation. Nevertheless, we show that such scenario is peculiar and impacting solutions are stable only in the narrow range of the controlling parameters. In view of these results, we confirm that by adjusting the coupling parameters we are able to control the system.

All the impacting solutions are stable in a narrow range of the parameter space, with a remarkably different system evolution. Hence, there is no universal scenario for all the considered states. The common part is the occurrence of a grazing bifurcation followed by an immediate second grazing-induced bifurcation which destroys the stability of the impacting solution. Our results prove that the destabilization of impacting solutions via soft impacts is robust and that it always occurs via grazing-induced bifurcations.

Acknowledgement

The first author has been supported by a Georg Forster Research Fellowship granted by the Alexander von Humboldt Foundation, Germany. PB is supported by the Foundation for Polish Science (FNP).

References

[1] G. Gilardi, I. Sharf, Literature survey of contact dynamics modelling, Mech. Mach. Theory 37 (10) (2002) 1213–1239.
[2] S.W. Shaw, P. Holmes, A periodically forced piecewise linear oscillator, J. Sound Vib. 90 (1) (1983) 129–155.
[3] U. Andreaus, L. Placidi, G. Rega, Numerical simulation of the soft contact dynamics of an impacting bilinear oscillator, Commun. Nonlinear Sci. Numer. Simul. 15 (9) (2010) 2603–2616.
[4] W. Goldsmith, Impact, the Theory and Physical Behavior of Colliding Solids. Ltd, Edward Arnold Pub, London, 1964.
[5] W. Serweta, A. Okolewski, B. Blazejczyk-Okolewska, K. Czolczynski, T. Kapitaniak, Lyapunov exponents of impact oscillators with hertz's and newton's contact models, Int. J. Mech. Sci. 89 (2014) 194–206.
[6] F. Peterka, Behaviour of impact oscillator with soft and preloaded stop, Chaos, Solitons Fractals 18 (1) (2003) 79–88.
[7] B. Banerjee, A. Bajaj, P. Davies, Resonant dynamics of an autoparametric system: A study using higher-order averaging, Int. J. Non-Linear Mech. 31 (1) (1996) 21–39.
[8] M. Bernardo, C. Budd, A.R. Champneys, P. Kowalczyk, Piecewise-smooth dynamical systems: theory and applications 163, Springer, 2008.
[9] A. Ganguli, S. Banerjee, Dangerous bifurcation at border collision: When does it occur*, Phys. Rev. E 71 (5) (2005) 057202.
[10] Y. Ma, M. Agarwal, S. Banerjee, Border collision bifurcations in a soft impact system, Phys. Lett. A 354 (4) (2006) 281–287.
[11] P. Brzeski, E. Pavlovskaia, T. Kapitaniak, P. Perlikowski, Controlling multistability in coupled systems with soft impacts, International Journal of Mechanical Sciences, 2016. http://dx.doi.org/10.1016/j.ijmecsci.2016.12.022.
[12] M. di Bernardo, C.J. Budd, A.R. Champneys, P. Kowalczyk, Piecewise-smooth dynamical systems Theory and Applications 163 of Applied Mathematical Sciences, Springer-Verlag, New York, 2004.
[13] L.F. Shampine, I. Gladwell, R.W. Brankin, Reliable solution of special event location problems for ODEs, CM Trans. Math. Softw. 17 (1) (1991) 11–25.
[14] L.F. Shampine, S. Thompson, Event location for ordinary differential equations, Comput. Math. Appl. 39 (5–6) (2000) 43–54.
[15] P.T. Piiroinen, Y.A. Kuznetsov, An event-driven method to simulate Filippov systems with accurate computing of sliding motions, ACM Trans. Math. Softw. 34 (2) (2008) 24.
[16] B. Krauskopf, H. Osinga, and J. Galan-Vioque, eds., Numerical Continuation Methods for Dynamical Systems. Understanding Complex Systems, Netherlands: Springer-Verlag 2007.
[17] F. Dercole, Y.A. Kuznetsov, SlideCont: an Auto97 driver for bifurcation analysis of Filippov systems, ACM Trans. Math. Softw. 31 (1) (2005) 95–119.
[18] P. Thota, H. Dankowicz, TC-HAT: A Novel toolbox for the continuation of periodic trajectories in hybrid dynamical systems, SIAM J. Appl. Dyn. Syst. 7 (4) (2008) 1283–1322.
[19] J. Páez Chávez, M. Wiercigroch, Bifurcation analysis of periodic orbits of a non-smooth Jeffcott Rotor Model, Commun. Nonlinear Sci. Numer. Simul. 18 (9) (2013) 2571–2580.
[20] J. Páez Chávez, E.E. Pavlovskaia, M. Wiercigroch, Bifurcation analysis of a piecewise-linear impact oscillator with drift, Nonlinear Dyn. 77 (1–2) (2014) 213–227.
[21] M. Liao, J. Ing, J. Páez Chávez, M. Wiercigroch, Bifurcation techniques for stiffness identification of an impact oscillator, Commun. Nonlinear Sci. Numer. Simul. 41 (2016) 19–31.
[22] J. Páez Chávez, Y. Liu, E.E. Pavlovskaia, M. Wiercigroch, Path-following analysis of the dynamical response of a piecewise-linear capsule system, Commun. Nonlinear Sci. Numer. Simul. 37 (2016) (2016) 102–114.
[23] J. Páez Chávez, A. Voigt, J. Schreiter, U. Marschner, S. Siegmund, A. Richter, A new self-excited chemo-fluidic oscillator based on stimuli-responsive hydrogels: Mathematical modeling and dynamic behavior, Appl. Math. Model. 20 (23–24) (2016) 9719–9738.
[24] H. Dankowicz, F. Schilder, Recipes for Continuation Computational Science and Engineering, SIAM, Philadelphia, 2013.
[25] H. Dankowicz, F. Schilder, An extended continuation problem for bifurcation analysis in the presence of constraints, J. Comput. Nonlinear Dyn. 6 (3) (2011) 031003.
[26] E.J. Doedel, A.R. Champneys, T.F. Fairgrieve, Y.A. Kuznetsov, B. Sandstede, and X.-J. Wang, Auto97: Continuation and bifurcation software for ordinary differential equations (with HomCont), Computer Science, Concordia University, Montreal, Canada, 1997.
[27] A. Dhooge, W. Govaerts, Y.A. Kuznetsov, MATCONT: A MATLAB package for numerical bifurcation analysis of ODEs, ACM Trans. Math. Softw. 29 (2) (2003) 141–164.
[28] Y.A. Kuznetsov, Elements of Applied Bifurcation Theory 112 Applied Mathematical Sciences, third ed, Springer-Verlag, New York, 2004.
[29] M. di Bernardo, C.J. Budd, A.R. Champneys, P. Kowalczyk, A. Nordmark, G. Tost, P.T. Piiroinen, Bifurcations in nonsmooth dynamical systems, SIAM Rev. 50 (4) (2008) 629–701.